Numerical investigation of the radial quadrupole and scissors modes in trapped gases

2012 EPL 97 16003

(http://iopscience.iop.org/0295-5075/97/1/16003)

A Letters Journal Exploring the Frontiers of Physics

January 2012

EPL, **97** (2012) 16003
doi: 10.1209/0295-5075/97/16003

www.epljournal.org

Numerical investigation of the radial quadrupole and scissors modes in trapped gases

Lei Wu and Yonghao Zhang[a]

Department of Mechanical and Aerospace Engineering, University of Strathclyde - Glasgow, G1 1XJ, UK, EU

received 5 September 2011; accepted in final form 21 November 2011
published online 3 January 2012

PACS 67.85.De – Dynamic properties of condensates; excitations, and superfluid flow
PACS 51.10.+y – Kinetic and transport theory of gases
PACS 05.20.Dd – Kinetic theory

Abstract – The analytical expressions for the frequency and damping of the radial quadrupole and scissors modes, as obtained from the method of moments, are limited to the harmonic potential. In addition, the analytical results may not be sufficiently accurate as an average relaxation time is used and the high-order moments are ignored. Here, we numerically solve the Boltzmann model equation in the hydrodynamic, transition, and collisionless regimes to study mode frequency and damping. When the gas is trapped by the harmonic potential, we find that the analytical expressions underestimate the damping in the transition regime. Furthermore, we demonstrate that the numerical simulations are able to provide reasonable predictions for the collective oscillations in the Gaussian potentials. The present method can also be used to study many other problems, *e.g.* formation of quantum shockwave, expansion of atom cloud, and effective heat conductivity in very elongated traps.

Introduction. – The realization of quantum degeneracy in the ultracold atomic gases has attracted intensive research efforts to understand the interacting quantum systems [1,2]. The experimental controllability of the interactions, energy, and spin population makes these systems ideal to study the crossover from a Bose-Einstein condensation (BEC) to a Bardeen-Cooper-Schrieffer (BCS) superfluid, which is ubiquitous in high-temperature superconductivity, neutron stars, nuclear matter, and quark-gluon plasma [3]. And the study of the low-lying excitation modes is important for probing the properties of strongly correlated systems, revealing the underlying mechanics of BEC-BCS crossover.

In the zero-temperature limit, the superfluid behavior of the quantum Fermi gases is well understood [2,4,5]. At high temperatures, the dilute quantum gases are in the normal phase and their dynamics can be described by the semi-classical Boltzmann equation [6]. On the other hand, when the temperature is below the critical temperature for superfluidity, the superfluid and normal phases coexist. In this case, the Boltzmann equation for the dynamics of the quasiparticle distribution function and the Euler equations for the superfluid order parameter can be combined to describe the quantum gas dynamics [7,8]. So far, however, the effects of temperature on the collective modes remain unclear. For instance, experimentally, in the same temperature range, Kinast *et al.* showed that the frequency of the radial compression mode stayed close to the hydrodynamic value [9], while Wright *et al.* measured the scissors mode and found a clear transition from the hydrodynamic to collisionless behavior [10]. This discrepancy motivated Riedl *et al.* to measure the frequency and damping of the radial compression, quadrupole, and scissors modes in a similar experimental condition and to compare the experimental data with the analytical prediction of the moment method [11]. However, there are discrepancies between the experimental and theoretical results, especially for the radial quadrupole mode.

The analytical expressions for the mode frequency and damping were obtained by applying the method of moments to the linearized Boltzmann equation [11–15]. However, the analytical method of moments may not provide accurate predictions for the two-component Fermi gases in the transition regime [11,16], which is caused by i) the spatially dependent relaxation time is replaced by the spatially average one and/or ii) only low orders of moments are included in the analytical method, which may not be adequate for capturing the important features

[a] E-mail: yonghao.zhang@strath.ac.uk

of the collective oscillations. For example, one needs to consider high-order terms for the cloud surface deformation at large radii in the quadrupole mode if using average relaxation time [16]. The other major drawback of the analytical method is that it is only limited to the external harmonic potentials, while experimentally anharmonic effects emerge at high temperatures where the external potential has a Gaussian profile [10,11]. Therefore, it is necessary to solve the Boltzmann equation numerically to get the accurate mode frequency and damping, which is the aim of the present paper.

Here we put forward a deterministic method to numerically solve the Boltzmann model equation in the hydrodynamic, transition, and collisionless regimes. We extract the frequency and damping of the radial quadrupole and scissors modes and compare them with the analytical and experimental data [10,11,13,15]. The numerical results agree better with the experimental data than the analytical results reported in refs. [10,11].

Model equation. – We consider two-component balanced Fermi gases well above the degeneracy temperature, where the gases are statistically classical but the collisions are quantum. The dilute Fermi gas is in the normal phase and the up-spin and down-spin components have the same atom mass m. Due to the Pauli's exclusion principle, collision happens between atoms with different spins. For most of the experiments the two components move together and one needs only consider one distribution function. Furthermore, the experiments of Wright *et al.* and Riedl *et al.* were conducted in elongated traps so that one can focus only on the radial collective oscillations, neglecting the axial motion [10,11,17]. Thus, the problem is effectively two-dimensional. In general, due to the presence of the Gaussian laser beam, the gas is trapped in the two-dimensional Gaussian potential

$$V(x,y)=V_0\left[1-\exp\left(-\frac{x^2}{a^2}-\frac{y^2}{b^2}\right)\right], \tag{1}$$

where V_0 is trap depth and a, b are the trap widths. However, at low temperatures, the size of atom cloud is far smaller than the trap widths. In this case, the external potential is nearly harmonic

$$V(x,y)=\frac{m}{2}(\omega_x^2x^2+\omega_y^2y^2), \tag{2}$$

where the trap frequencies satisfy $\Omega_x=\sqrt{2V_0/m}/a$ and $\Omega_y=\sqrt{2V_0/m}/b$.

Instead of the Boltzmann equation, we begin with the kinetic model equation based on the relaxation-time approximation; this model can capture the essential physics of the problem and has been widely used to describe the rarefied gas dynamics [18]. It reads

$$\frac{\partial f}{\partial t}+v_x\frac{\partial f}{\partial x}+v_y\frac{\partial f}{\partial y}+a_x\frac{\partial f}{\partial v_x}+a_y\frac{\partial f}{\partial v_y}=\frac{f_{le}-f}{\tau(x,y)}, \tag{3}$$

where $f(x,y,v_x,v_y;t)$ is the reduced distribution function which neglects the axial motion, v_x and v_y are velocity components, $(a_x,a_y)=-(\partial/\partial x,\partial/\partial y)V/m$ are the accelerations, $\tau(x,y)$ is the local relaxation time, and f_{le} is the local equilibrium distribution function

$$f_{le}=\frac{mn}{2\pi k_BT}\exp\left[-m\frac{(v_x-u_x)^2+(v_y-u_y)^2}{2k_BT}\right], \tag{4}$$

which is defined in terms of the local particle density $n(x,y)$, local temperature $T(x,y)$, local macroscopic velocities $u_x(x,y)$ and $u_y(x,y)$, and the Boltzmann constant k_B. When the system is in global thermal equilibrium, $n=n_0\exp[-V(x,y)/k_BT_0]$, with n_0 being the particle density at the trap center and T_0 the global equilibrium temperature.

The relaxation time can be determined by macroscopic properites such as shear viscosity or by microscopic information. The shear viscosity plays a dominant role in the collective oscillations; the atom cloud remains nearly isothermal and the experiment is not sensitive to the thermal conductivity [19,20]. Therefore, the local relaxation time can be determined by equating the shear viscosity with that derived from the kinetic model equation (3), yielding $\tau=\eta/nk_BT$. Using microscopic information, we have $\tau(x,y)=15\sqrt{m\pi/k_BT}/16\sigma n\int_0^\infty \mathrm{d}\xi\xi^7e^{-\xi^2}(1+\xi^2T/T_a)^{-1}$, where $\sigma=4\pi a^2$ is the total energy-independent cross-section and $T_a=\hbar^2/mk_Ba^2$, with a the s-wave scattering length and $\hbar$ the Planck constant [14]. Two limiting cases will be considered. When a is small, the scattering cross-section is energy-independent, and atoms behave like hard spheres. The local relaxation time is therefore given by [14,21,22]

$$\tau(x,y)=\frac{5}{16\sigma n(x,y)}\sqrt{\frac{m\pi}{k_BT(x,y)}}. \tag{5}$$

In the unitarity limit where $a\to\infty$, we have

$$\tau(x,y)=\frac{15m^{3/2}}{64\hbar^2n(x,y)}\sqrt{\frac{k_BT(x,y)}{\pi}}. \tag{6}$$

Numerical scheme. – The relaxation time is a crucial parameter in the collective oscillations. A spatially uniform gas is in the hydrodynamic regime when $\omega_0\tau\ll1$. Here ω_0 is the external trap frequency (the mode frequency is of the same order). In this circumstance, the Euler and Navier-Stokes equations can be derived from the Boltzmann equation by the Chapman-Enskog expansion [21]. On the contrary, the gas is collisionless when $\omega_0\tau\gg1$. When the gas is trapped, however, it could be in the hydrodynamical, transition ($\omega_0\tau\sim1$), or collisionless regime in the central region of the trap, whereas in the surface region it is always collisionless. The different order-of-magnitude of τ across the trap poses difficulty in numerical simulations: if one wants to resolve the details of the collision, the time step Δt should be smaller than τ, which is not practical for the long time behavior when the gas is in the hydrodynamic regime ($\tau\to0$). Therefore, in a calculation, it is desirable

to use a numerical scheme that can have practical time step across hydrodynamic and collisionless regimes as we are interested in the macroscopic behavior of the gas.

In order to have practical time step in hydrodynamic regime where τ is small, we adopt the concept of asymptotic preserving to solve the model equation (3) numerically [23,24]. The virtue of this scheme is that it can capture the macroscopic gas dynamics in the hydrodynamic limit even if the small scale determined by the relaxation time τ is not numerically resolved. The computational accuracy in the hydrodynamic regime is guaranteed by the fact that, using the Chapman-Enskog expansion [25], this numerical scheme yields the correct Euler equations when τ goes to zero while the spatial and time steps are fixed. Therefore, the computation of a hydrodynamic flow can be as fast and accurate as that of the transition and collisionless flows. This unique feature cannot be implemented by the probabilistic methods such as the direct simulation Monte Carlo and molecular dynamics simulation.

The terms at the left side of eq. (3) are treated explicitly, while the collision term at the right side is treated implicitly to overcome its stiffness in the hydrodynamic regime (the stiff means that, since $\tau(x,y)\to 0$, numerical errors can be greatly amplified), yielding

$$\frac{f^{j+1}-f^{j}}{\Delta t}+Tr[f^{j}]=\frac{1}{\tau^{j+1}(x,y)}(f_{le}^{j+1}-f^{j+1}), \qquad (7)$$

where variables with superscript j denote the values of these variables at the j-th time step and $Tr[f^j]$ represents the spatial and velocity discretization of the last four terms at the left side of eq. (3). If the spatial and velocity ranges are wide enough, f is zero at the boundaries, so that $Tr[f^j]$ can be handled by the fast Fourier transformation. By using the conservative properties of the collision term, the nonlinear implicit equation (7) can be solved explicitly. That is, given f^j, one can get n^{j+1}, u_x^{j+1}, u_y^{j+1}, and T^{j+1} from the following equations: $n^{j+1}=\int F\mathrm{d}v_x\mathrm{d}v_y$, $(u_x^{j+1},u_y^{j+1})=\int(v_x,v_y)F\mathrm{d}v_x\mathrm{d}v_y/n^{j+1}$, and $T^{j+1}=m[\int(v_x^2+v_y^2)Fdv_xdv_y/n^{j+1}-(u_x^{j+1})^2-(u_y^{j+1})^2]/2k_B$, where $F=f^j-\Delta tT[f^j]$ and the numerical integration can be carried out by direct discrete sum or by the Simpson's rule. The above four macroscopic quantities at the $(j+1)$-th time step determine f_{le}^{j+1} according to eq. (4) and τ^{j+1} according to eq. (5) or (6). Therefore, f^{j+1} can be solved explicitly.

In practice, since $n(x,y)$ is very small near the boundary, numerical error emerges when calculating the macroscopic velocity. Hence it is possible to get negative temperature, which is not physical. To tackle this problem, the collision term in eq. (7) is neglected near the spatial boundary. This is justified by the fact that far from the trap center the gas is in the collisionless limit so the collision term is negligible. Another point one should pay attention to is that, the maximum Courant-Friedrichs-Lewy (CFL) number

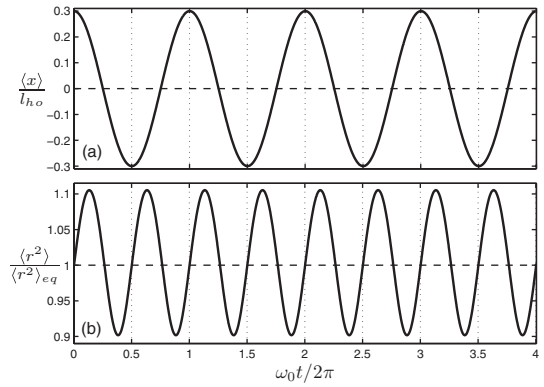

Fig. 1: Numerical simulation of the radial (a) sloshing mode and (b) breathing mode. The initial distribution function is $f=\exp\{-[\omega_0^2(x-0.3l_{ho})^2+\omega_0^2y^2+v_x^2+v_y^2]/2\}/2\pi$ for the sloshing mode and $f=\exp\{-[\omega_0^2(x^2+y^2)+(v_x-0.8x)^2+(v_y-0.8y)^2]/2\}/2\pi$ for the breathing mode. In both simulations, $m=k_B=T_0=1,\omega_0=\sigma=4$, so that the characteristic length l_{ho} is 0.25 and the system is in the transition regime. The spatial region $[-1.5,1.5]\times[-1.5,1.5]$ and the velocity region $[-8,8]\times[-8,8]$ are uniformly discretized into 64×64 and 32×32 meshes, respectively. The time step is $\Delta t=0.002$ and the maximum CFL number is 0.875.

$\Delta t\cdot max\{|v_x|/\Delta x+|v_y|/\Delta y+|a_x|/\Delta v_x+|a_y|/\Delta v_y\}$ with $\Delta x,\Delta y$ the spatial steps and $\Delta v_x,\Delta v_y$ the velocity steps, must be smaller than 1.

Numerical results for the harmonic potential. – To validate the numerical scheme, we simulate the radial sloshing and breathing modes in the isotropic harmonic trap with $\omega_x,\omega_y=\omega_0$. The local relaxation time is given by eq. (5). However, the use of eq. (6) will give the same result because the cloud is nearly isothermal, *i.e.*, after normalization, only $n(x,y)$ affects $\tau(x,y)$. The numerical results in fig. 1 show that, as expected, the sloshing and breathing modes oscillate with the frequency ω_0 and $2\omega_0$, respectively [12,16]. Note that the simulations were carried out in the transition regime, where damped modes are suppressed rapidly. The two perfectly undamped modes prove the accuracy of the numerical scheme.

Now we simulate the radial quadrupole mode and compare the results with the analytical and experimental ones. Analytically, replacing the local relaxation time by the average relaxation time $\widetilde{\tau}=2\sqrt{2}\tau(0,0)$ and applying the method of moments up to the second-order, one find that the mode frequency ω_r and damping rate ω_i satisfy [13,26]

$$\omega^2-2\omega_0^2-i\omega\widetilde{\tau}(\omega^2-4\omega_0^2)=0, \qquad (8)$$

where $\omega=\omega_r-i\omega_i$. This equation clearly shows that in the hydrodynamic regime, the mode frequency is $\Omega_r=\sqrt{2}\Omega_0$, while in the collisionless regime, it is $\omega_r=2\omega_0$.

As mentioned above, the analytical solution (8) are not accurate due to the local relaxation time is replaced by the average one and/or only the second-order moments are included. To see which factor affects the accuracy of

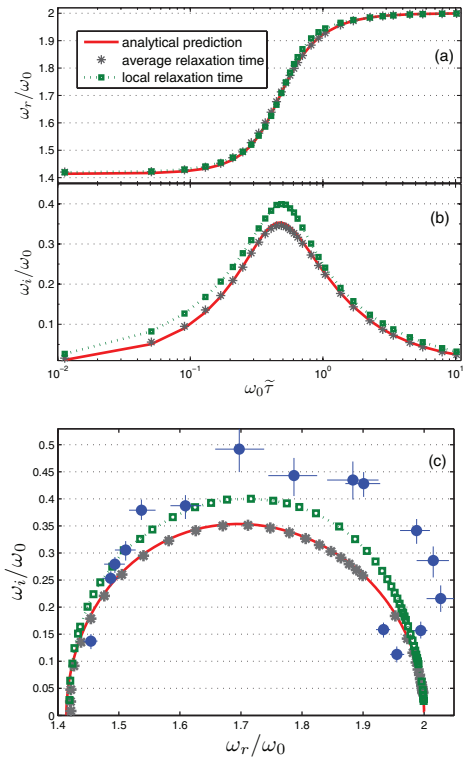

Fig. 2: (Color online) (a) The normalized collective frequency and (b) damping of the radial quadrupole mode *vs.* the nondimensional variable $\Omega_0\widetilde{\tau}$. The results are obtained by fitting the quadrupole moment $Q=\langle x^2-y^2\rangle$ through the equation $Q(t)=A\exp(-\omega_i t)\sin(\omega_r t+\phi)+B\exp(-Ct)$. The quadrupole mode is excited by initial distribution function $\exp\{-[\omega_0^2(x^2+y^2)+(v_x-0.8x)^2+(v_y+0.8y)^2]/2\}/2\pi$. The value of cross-section σ is varied to change the system from the hydrodynamic limit to the collisionless limit. Other parameters are the same as those in fig. 1. (c) Damping ω_i *vs.* collective frequency ω_r of the radial quadrupole mode. For the experimental data (solid circles), ω_0 represents the frequency of the sloshing mode when the gas is trapped in the Gaussian potential [11].

the analytical results, we use both the local and average relaxation times in the numerical simulations. Numerically extracted mode frequency and damping are depicted in fig. 2. When the average relaxation time is used, the numerically obtained mode frequency, damping, and their relations (stars) agree with the analytical results very well, indicating that it is sufficient to include up to the second-order moments. The inaccuracy of the analytical results is therefore caused solely by replacing the local relaxation time with the average one. Comparing the analytical results with the numerical (squares, when the local relaxation time is used) and experimental ones (solid circles), one finds that the analytical mode frequency coincides with the numerical one (fig. 2(a)), while the analytical method underestimates the damping, especially in the transition regime (fig. 2(b) and (c)). The numerical results (squares) agree better with the experimental data than the analytical results reported in refs. [11].

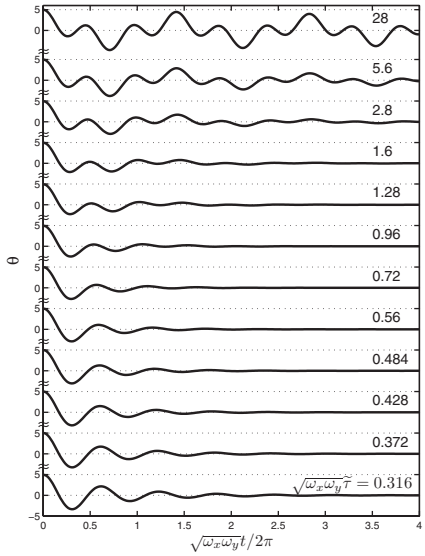

Fig. 3: The angle (in degrees) of atom cloud *vs.* the normalized time. The scissors mode is excited by sudden rotation of the trap angle $\theta(0)$ by 5°. The trap frequencies are $\omega_x=2\omega_y=4$. The time step is $\Delta t=0.0025$ and the maximum CFL number is 0.82. The other parameters are the same as those in fig. 1, except the spatial region in the y-direction is now $[-3,3]$. The angle is obtained by $\theta(t)=90\mathrm{atan}[\langle xy\rangle/\langle x^2-y^2\rangle]/\pi$.

Finally, we simulate the radial scissors mode in the elliptical harmonic potential with $\omega_x=2\omega_y=4$. Analytically, the method of moments up to second-order predicts the following relation between the mode frequency and damping [15]

$$i\omega(\omega^2-\omega_h^2)+\widetilde{\tau}(\omega^2-\omega_{c1}^2)(\omega^2-\omega_{c2}^2)=0, \qquad (9)$$

where $\omega_h=(\omega_x^2+\omega_y^2)^{1/2}$ is the frequency in the hydrodynamic limit and $\omega_{c1}=\omega_x+\omega_y$, $\omega_{c2}=|\omega_x-\omega_y|$ are the frequencies at the collisionless limit.

Typical oscillation sceneries of the radial scissors mode are shown in fig. 3. In the collisionless limit ($\sqrt{\Omega_x\Omega_y}\widetilde{\tau}=28$), the angle of atom cloud oscillates with two frequencies of 5.999 and 2, and the damping rate of 0.036. As the value of $\sqrt{\Omega_x\Omega_y}\widetilde{\tau}$ decreases, both the frequencies decrease, with the larger one gradually reducing to $2\sqrt{2}$ (fig. 4(a)) and the smaller one quickly approaching zero. For example, when $\sqrt{\Omega_x\Omega_y}\widetilde{\tau}=0.316$, $\omega_r=4.609$ and the smaller frequency is already 0.012; however, the damping corresponding to the larger frequency decreases with an initial increase (fig. 4(b)). The largest damping is achieved when $\sqrt{\Omega_x\Omega_y}\widetilde{\tau}=0.72$, where the scissors mode damps out within 2 oscillations. When the average relaxation time is used in the numerical simulation, the mode frequency (stars) overlaps with the analytical prediction (fig. 4(a)), while the damping agrees with the analytical prediction only in the hydrodynamic and collisionless regimes (fig. 4(b)); in the transition regime the damping is slightly larger than that of the analytical prediction. This implies that, unlike the radial quadrupole mode, the

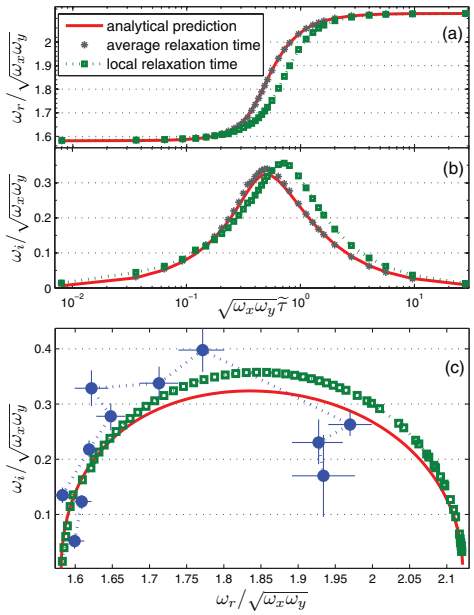

Fig. 4: (Color online) The normalized (a) collective frequency and (b) damping rate of the radial scissors mode *vs.* the average relaxation time. The results are obtained by fitting the cloud angle to a sum of two damped sine functions each with their own free parameters. Only the higher frequency and the corresponding damping rate is plotted. (c) Damping ω_i *vs.* collective frequency ω_r of the radial scissors mode. Experimental data (solid circles) are collected from ref. [10].

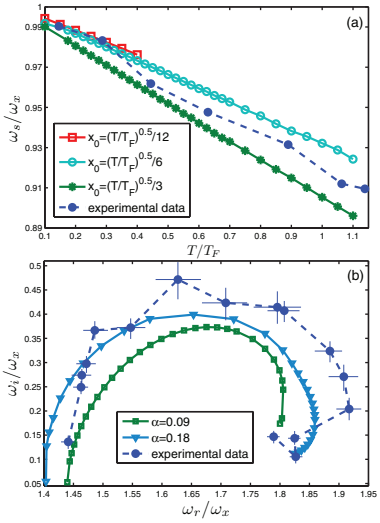

Fig. 5: (Color online) (a) The sloshing mode frequency *vs.* the temperature in the Gaussian potential. (b) Damping rate ω_i *vs.* collective frequency ω_r of the radial quadrupole mode. The spatial region $[-\sqrt{\widetilde{T}},\sqrt{\widetilde{T}}]\times[-\sqrt{\widetilde{T}},\sqrt{\widetilde{T}}]$ and the velocity region $[-8\sqrt{\widetilde{T}},8\sqrt{\widetilde{T}}]\times[-8\sqrt{\widetilde{T}},8\sqrt{\widetilde{T}}]$ are uniformly discretized into 64×64 and 32×32 meshes, respectively. The time step is $\Delta t=0.0013$.

analytical ansatz (see eq. (4) in ref. [15]) is not accurate enough. When the local relaxation time is used, both the mode frequency and damping do not agree with the analytical prediction, especially in the transition regime: the mode frequency is always larger than the analytical one, while the damping could be smaller or larger than the analytical one, depending on the value of $\sqrt{\Omega_x\Omega_y}\widetilde{\tau}$. For the relation between mode frequency and damping, the numerical results are always larger than the analytical one, see fig. 4(c). Like the radial quadrupole, the numerical results are closer to the experimental data than the analytical results at low temperatures. At higher temperatures, the anharmonic effect of the external Gaussian potential becomes important, and there are large errors in the frequency and damping, see the last three experimental data in fig. 4(c).

Numerical results for the Gaussian potential. – Instead of the harmonic potential, the gases are trapped in the Gaussian potential at higher temperatures. The moment method fails to provide analytical solution for the Gaussian potential, so we have to rely on numerical simulations. To calculate the collective frequency and damping of the radial quadrupole mode, the following experimental data are used [11]: $V_0=50k_B$ μK, $a,b=32.8\,\mu$m, with the corresponding trap frequency $\omega_x,\omega_y=1800\times2\pi$ Hz. The trap frequency in the z direction is $\omega_z=32\times2\pi$ Hz, and the total number of atoms is $N=6\times10^5$. In numerical simulations, the time, spatial coordinates, velocity, and temperature are respectively normalized by $a\sqrt{m/k_BT_F}$, a, $\sqrt{k_BT_F/m}$, and the Fermi temperature $T_F=2.73\,\mu$K. The distribution function is also normalized by the particle density at the trap center. Therefore, the normalized accelerations in the x and y directions are respectively $-36.6x\exp(-x^2-y^2)$ and $-36.6y\exp(-x^2-y^2)$, and at the unitarity limit, the normalized local relaxation time is $\tau(x,y)=0.09(T/T_F)^2/n(x,y)$.

Figure 5(a) shows the frequency of the sloshing mode decreases as the temperature increases, which coincides with the experimental observations. This can be explained by the fact that the anharmonicity becomes stronger and stronger as the cloud size increases due to the temperature rise. Also, we find that the frequency decreases as the cloud's initial center x_0 increases. Note that the sloshing mode is excited by shifting the Gaussian potential by x_0 in the x direction.

Figure 5(b) demonstrates the relation between the mode frequency and damping, where the local relaxation time is $\tau(x,y)=\alpha\widetilde{T}^2/n(x,y)$, the initial distribution function is $f=\exp\{-18.3[1-e^{-x^2/1.05^2-1.05^2y^2}]/\widetilde{T}\}\exp[-(v_x^2+v_y^2)/2\widetilde{T}]/2\pi\widetilde{T}$, and $\widetilde{T}=T/T_F$. In the numerical simulation we use two values of α, because if the repulsive mean-field potential is presented in the experiment, the atom density at the trap center will decrease and hence the coefficient will be larger than 0.09. When $\alpha=0.09$, as the temperature increases (corresponding to the data from left to right), the mode frequency first increases, remains almost unchanged at $\omega_r/\omega_x\approx1.8$, and then slightly decreases. The constant frequency is due to the balance between

the anharmonic and collisionless effects: the anharmonic effect reduces the effective trap frequency (and hence the mode frequency) while the collisionless effect increases the mode frequency. When $\alpha = 0.18$, the trend of the relation between the mode frequency and damping agrees with the experimental finding reasonably well. That is, from the hydrodynamic regime to the collisionless regime, the mode frequency first increases and then decreases. These results indicate that our numerical scheme can provide reasonable predictions for the collective oscillations in the Gaussian potentials. Also, it indicates that the difference between the numerical and experiment results may be a consequence of the approximation of the relaxation rate or the neglected mean-field potential term in eq. (3), rather than the anharmonic effect [11].

Outlook. – In summary, to improve the accuracy and overcome the limitation of the method of moments, we have demonstrated a computationally efficient numerical scheme to solve the Boltzmann model equation. The extracted mode frequency and damping of the radial quadrupole and scissors modes provide better agreement with the experimental data than the analytical solutions obtained from the method of moments. The advantage of this numerical approach is that it can deal with the harmonic and Gaussian potentials, as well as other forms of the potential, including the mean-field and other self-energy terms, which will help us to understand the properties of strongly interacting particles. In particular, the asymptotic preserving nature of the numerical scheme makes the computation of a hydrodynamic flow as fast and accurate as that of the transition and collisionless flows, which cannot be implemented by the probabilistic methods.

In addition to the study of collective oscillations, the present method can be useful for investigation of many other problems. For example, one can use it to study the expansion of the atom cloud after the trap being switched off; to examine the collision of two initially separated atom clouds to see the formation of quantum shock waves [27]; to determine the effective transport coefficients such as the heat conductivity in very elongated traps [28]. Furthermore, the deterministic nature of the numerical scheme makes it suitable to solve the two-fluid equation, one for the normal phase and the other for the superfluid phase [7]. So the numerical simulations will help us to understand the coupled dynamics of the superfluid and normal phases, *i.e.*, the damping of superfluid flow by a thermal cloud [29].

* * *

The authors would like to thank the referees for their helpful suggestions.

REFERENCES

[1] Dalfovo F., Giorgini S., Pitaevskii L. P. and Stringari S., *Rev. Mod. Phys.*, **71** (1999) 463.
[2] Giorgini S., Pitaevskii L. P. and Stringari S., *Rev. Mod. Phys.*, **80** (2008) 1215.
[3] Cao C. *et al.*, *Science*, **331** (2011) 58.
[4] Menotti C., Pedri P. and Stringari S., *Phys. Rev. Lett.*, **89** (2002) 250402.
[5] Cozzini M. and Stringari S., *Phys. Rev. Lett.*, **91** (2003) 070401.
[6] Uehling E. A. and Uhlenbeck G. E., *Phys. Rev.*, **43** (1933) 552.
[7] Jackson B. and Zaremba E., *Phys. Rev. Lett.*, **88** (2002) 180402.
[8] Urban M. and Schuck P., *Phys. Rev. A*, **73** (2006) 013621.
[9] Kinast J., Turlapov A. and Thomas J. E., *Phys. Rev. Lett.*, **94** (2005) 170404.
[10] Wright M. J. *et al.*, *Phys. Rev. Lett.*, **99** (2007) 150403.
[11] Riedl S. *et al.*, *Phys. Rev. A*, **78** (2008) 053609.
[12] Guéry-Odelin D., Zambelli F., Dalibard J. and Stringari S., *Phys. Rev. A*, **60** (1999) 4851.
[13] Al Khawaja U., Pethick C. J. and Smith H., *J. Low Temp. Phys.*, **118** (2000) 127.
[14] Massignan P., Bruun G. M. and Smith H., *Phys. Rev. A*, **71** (2005) 033607.
[15] Bruun G. M. and Smith H., *Phys. Rev. A*, **76** (2007) 045602.
[16] Lepers T., Davesne D., Chiacchiera S. and Urban M., *Phys. Rev. A*, **82** (2010) 023609.
[17] Altmeyer A. *et al.*, *Phys. Rev. A*, **76** (2007) 033610.
[18] Cercignani C., *Rarefied gas dynamics* (Cambridge University Press, Cambridge) 2000.
[19] Kavoulakis G. M., Pethick C. J. and Smith H., *Phys. Rev. A*, **57** (1998) 2938.
[20] Braby M., Chao J. and Schäfer T., *Phys. Rev. A*, **82** (2010) 033619.
[21] Nikuni T. and Griffin A., *J. Low Temp. Phys.*, **111** (1998) 793.
[22] Watabe S., Osawa A. and Nikuni T., *J. Low Temp. Phys.*, **158** (2010) 773.
[23] Jin S., *SIAM J. Sci. Comput.*, **21** (1999) 441.
[24] Filbet F. and Jin S., *J. Sci. Comput.*, **46** (2011) 204.
[25] Chapman S. and Cowling T. G., *The Mathematical Theory of Non-Uniform Gases* (Cambridge University Press, Cambridge) 1970.
[26] Buggle Ch., Pedri P., von Klitzing W. and Walraven J. T. M., *Phys. Rev. A*, **72** (2005) 043610.
[27] Joseph J. A., Thomas J. E., Kulkarni M. and Abanov A. G., *Phys. Rev. Lett.*, **106** (2011) 150401.
[28] Meppelink R., van Rooij R., Vogels J. M. and van der Straten P., *Phys. Rev. Lett.*, **103** (2009) 095301.
[29] Meppelink R., Koller S. B., Vogels J. M., Stoof H. T. C. and van der Straten P., *Phys. Rev. Lett.*, **103** (2009) 265301.